Aerosound from Corner Flow and Flap Flow

W. C. Meecham*
University of California, Los Angeles, California

The model consists of a vortex moving aound a corner in an incompressible, potential flow. A possible explanation of the typically small Strouhal numbers seen here is the vortex image retarding effect. The model surface pressures, sound pressures (using Curle's theory), and Mach number dependencies agree well with wind tunnel experiments. A double pressure peak is found in the model (credited to image action) which is qualitatively similar to measured sound correlations. Incompressible-flow aerosound calculations are discussed.

I. Introduction

RESIDENTS around airports are often exposed to high noise levels by commercial jet planes during landing operations. The problem is aggravated by small glide angles necessary during approach. (Although the noise produced at takeoff is much greater, it does not last as long at ground level because of higher climb-out angles.)

It is also true that, at landing, engines are operated at reduced thrust, and consequently high-lift airframe components, such as slots and flaps, may become noise sources of importance. Recent work by Ahtye et al.,[1] Fink and Schlinker,[2] and Kendall and Ahtye[3] has indicated that of the various possible airframe noise sources, the side edges of flaps seem to dominate. This is presumably because of the spanwise flow caused by the pressure differential between the high pressure, lower flap surface and the lower pressure, upper flap surface. The importance of this noise source is emphasized by the fact that the eddy structure in this side edge region shows a correlation length on the order of the flap chord, which is considerably greater than the typical turbulent eddy correlation lengths found elsewhere in the flow. Such larger correlation lengths enhance the radiated sound as will be seen below (see Refs. 4 and 5).

Earlier work[6] had emphasized as an important noise source region the trailing edges of flaps and wings. However, our measurements[1] indicate that the noise from the trailing edges of flaps is small (in our case undetectable) except at the very corners of the flap, inboard and outboard. Earlier, more extensive measurements by Yu and Tam[7] also indicated that such trailing edge noises were quite small. This result may be regretted, for it is clear that the geometry of a trailing edge is considerably simpler than that of separated flow around corners. In the latter case we must contend with swirling flows, corners, and other complications.

We present here a model problem calculation which we hope will be applicable to other problems involving the generation of aerosound by turbulent flow around corners. Our application is, of course, the flap edge, and we use the language of that problem.

To begin the treatment, we must first deal with the flow around a blunt object. One could construct an elaborate, empirical treatment for the discussion of aerosound from such flows; obviously a more analytical approach would be desirable. One simplified model for these flow processes involves the use of moving vortices imbedded in potential flows (for an inviscid, incompressible fluid). The main advantage here is that one has available conformal mapping procedures. The treatment leads naturally to a two-dimensional statement of the problem. This type of development forms only a model of the actual, very complicated flow problem.

The physical flow consists of distributed vorticity with all of the complexities inherent in the inhomogeneous turbulent process. If we are to make progress using an analytical treatment, a simpler model, such as described above is clearly needed. Among authors adopting such methods are Clements[8] for fluid mechanics, and Howe[9,10] and Hardin[11] for flow about a half-plane with application to aerosound. In Refs. 9 and 11 a special and simple procedure due to Howe is employed in the calculation. This procedure, if complete, permits a considerable simplification in the determination of the aerosound. However, if we use it, when the two-dimensional problem is adapted to three-dimensional geometries it appears that the sound power goes as the fourth power of the flow Mach number; as is known, Lighthill[12] finds for volume sound an eighth power of the Mach number and Curle[13] produces the well-known sixth-power dependence for surface sound. These apparent difficulties persuaded the author to carry out calculations here using standard Lighthill-Curle theory. As will be seen below, the surface sound yields a sixth-power dependence, with a dipole angular distribution.

A further difficulty with some earlier work is the following: In an exact theoretical statement of the problem, the fields for an incompressible flow should be recovered. Thus, if exactly incompressible quantities are used, one should find no radiated sound when including both volume and surface sound. That does not appear to be the case in the cited references. It is expected for the Lighthill-Curle theory that such a result should follow.

We propose to use incompressible flow quantities for the calculation of aerosound radiated by the flap surface.

In the standard treatment of the problem one finds sound radiated as a result of two source mechanisms, volume sound and surface sound. If we use the statement of the radiated sound in terms of density changes, then for incompressible flow these two integral contributions should be equal and opposite, since of course there is no density change in an incompressible fluid. In the course of the Lighthill-Curle discussion, what is really an arbitrary parameter, a_0, is introduced. It is convenient ordinarily to choose for that parameter the ambient speed of sound. For an incompressible flow problem we are free to make an arbitrary choice. If one does so, then the surface and volume sound must just cancel one another. We will here calculate the surface sound radiated by our model of the process. We do so using incompressible flow quantities. The rationale which we employ, and which is implicit in other similar treatments of the problem, is that the

Presented as Paper 81-2039 at the AIAA 7th Aeroacoustics Conference, Palo Alto, Calif., Oct. 5-7, 1981; submitted Oct. 28, 1981; revision received May 13, 1982. Copyright © 1981 by W. C. Meecham. Published by the American Institute of Aeronautics and Astronautics with permission.

*Professor, Department of Mechanics and Structures, School of Engineering and Applied Sciences. Associate Fellow AIAA.

field quantities near the surfaces producing dipole sound are approximately the same for an incompressible fluid and for a slightly compressible one under similar conditions. Thus we may use the simpler incompressible quantities in the calculation. These questions are discussed more fully in Appendix A.

Figure 1 shows a sketch of the wing and deployed flap, viewed from the underside of the wing. Two average streamlines are shown. Viewed from the aircraft, the flow proceeds along the wing and then spills (or is pushed by the high pressure on the underside of the flap) around the outboard blunt edge of the flap. Figure 2 is a closeup of the flow around this blunt edge and also shows the coordinate system used: The x_1 axis lies along the trailing edge of the flap; the x_3 axis lies along the outboard, lower edge of the flap; and x_2 is perpendicular to the underside of the flap. A field point $\boldsymbol{x}$ is shown. The dotted line from $\boldsymbol{x}$ is its projection on the x_1-x_2 plane, Φ is the (azimuthal) angle of that projection from the x_2 axis, and Θ is the polar angle, measured from the x_3 axis. Figure 3a shows the model, potential flow about the flap corner with an imbedded vortex. Figure 3b shows the uniform flow with the vortex (and its image) in the transformed plane (see below).

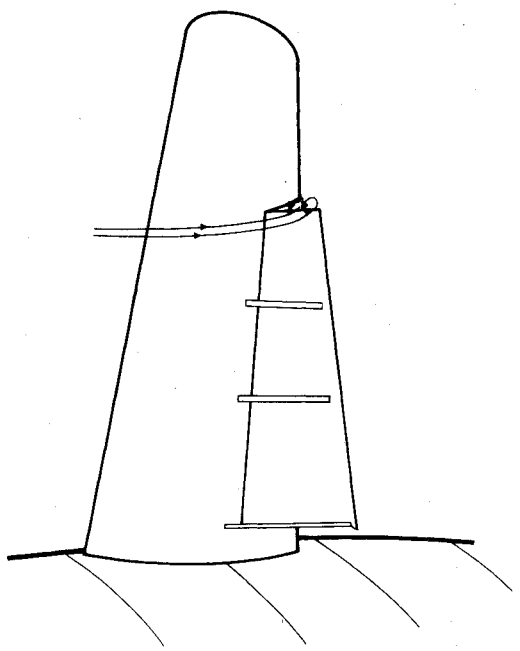

Fig. 1 Deployed flap, from the underside of the wing. Two average streamlines are indicated.

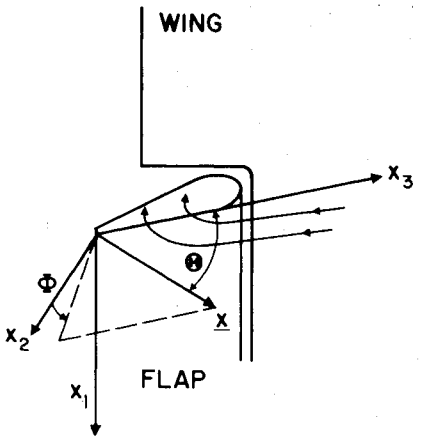

Fig. 2 Enlarged view of the deployed flap, with coordinate system indicated. The dashed line shows the projection of x in the x_1-x_2 plane.

In the spanwise flow about the blunt end of the flap, it was found in Refs. 1, 4, and 5 that most of the sound was radiated from the underside of the flap, that is, the surface on which the flow first impinges, the horizontal surface in Fig. 3a. This was determined through the use of cross-correlation techniques. The upper side of the flap showed little detectable, radiated sound. Our model here will consist of a vortex moving around from the lower horizontal surface to the vertical surface. We make no effort to construct the flow around the upper horizontal surface, the dashed line in Fig. 3a, for reasons just cited. Typically one thinks of flow separation at the corners producing vortices. In our case, from the cross-correlation measurements taken at the lower surface, it is clear that the vortex when formed is large enough and diffuse enough so that it has a major effect on the lower surface, thus not appearing *just* at the corner. The qualitative characteristics of the flow to be used here are similar to those measured around edges by Francis and Kennedy.[14] In our experiments we did not actually place pressure sensors at the blunt edge of the flap, in Fig. 3a the lower portion of the vertical surface. But we expect that when such experiments are performed, appreciable sound will be found originating from this region as well. We include it in our treatment.

II. Theory of Airframe Surface Noise

It is not necessary to review completely the standard aerosonic theory. We content ourselves with a few points of importance in the discussion and with results. Lighthill[12] beigns with the exact equations of motion for a fluid. In his treatment he models the propagation of sound in a fluid at rest. He has, at an intermediate stage,

$$\frac{\partial^2\rho}{\partial t^2} - a_0^2\nabla^2\rho = \frac{\partial^2}{\partial x_i \partial x_j} T_{ij} \qquad T_{ij} = \rho u_i u_j + p_{ij} - a_0^2\rho\delta_{ij} \quad (1)$$

where ρ is the density, p_{ij} the compressive stress tensor, a_0 the speed of sound in the ambient fluid (although a_0 may be chosen arbitrarily), and u_i the components of the fluid velocity in the direction x_i ($i=1,2,3$); we sum over repeated indices. Equation (1) is solved for free-turbulence flows by Lighthill and for turbulence in the presence of rigid boundaries by Curle.[13] For the surface contribution to the density change (in the situation where $x \gg \lambda \gg L$ with λ the wavelength of the most strongly radiated sound and L a typical dimension of the solid body of interest), Curle obtained the following:

$$x_i(4\pi a_0^3 x^2)^{-1}\frac{\partial}{\partial t}\int_s P_i\left(y, t-\frac{r}{a_0}\right)\mathrm{d}S(y) \quad (2)$$

where y is the source position vector, $r=|x-y|$, and x is the field point. The source system is said to be compact if $\lambda \gg L$. Below it is understood that the radiated signal is delayed by r/a_0; we shall not always show the delay explicity.

The P_i are the components of the force exerted by the surface on the surrounding fluid. The integral is to be carried

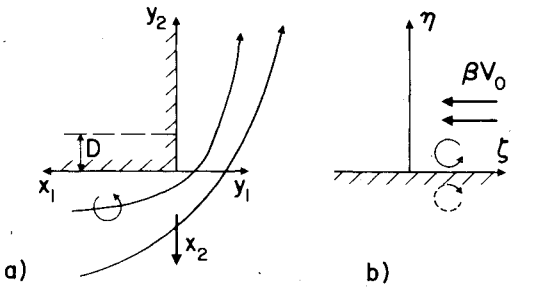

Fig. 3 a) Potential flow about a corner. The dashed line shows the nominal upper surface of the flap. A vortex is shown circulating with the potential flow. b) Uniform flow in the transformed plane.

out over the entire surface. For simplicity in our application we assume that the chord, C, is small compared with the sound wavelength and that we are far away compared with C. The dimension of the flap in the spanwise direction may be larger than the sound wavelength. However, our noise-producing eddies have a scale in the spanwise direction of order the thickness of the flap, see Refs. 1 and 4; it is known that the dipole sound vanishes for turbulence over a flat plate. Thus, far from the flap edge, we expect little surface-sound contribution. Consequently, we have assumed that the sources are compact for the entire radiating portion of the surface.

Our model consists of a vortex (plus its image) imbedded in a potential flow around a corner. We introduce a complex variable,

$$z=y_1+iy_2=Re^{i\theta} \qquad -\pi\leq\theta\leq\pi/2$$

Physical space may be transformed, as shown in Fig. 3b, with $\lambda=\xi+i\eta$, using

$$\lambda=(ze^{i\pi})^{2/3} \tag{3}$$

Assuming a uniform flow in the transformed plane, the complex potential is

$$W(\lambda)=-A\lambda-(i\Gamma/2\pi)\ell n(\lambda-\lambda_0)+(i\Gamma/2\pi)\ell n(\lambda-\lambda_0^*) \tag{4a}$$

Here $\lambda_0=\xi_0+i\eta_0$, the transformed vortex positions; A determines the magnitude of the uniform flow in the negative ξ direction; and the complex conjugate is indicated throughout by an asterisk. The Γ is the circulation strength of the vortex. Also $z_0=y_{01}+iy_{02}=R_0e^{i\theta_0}$ is the vortex position in the physical plane and is related to λ_0 by Eq. (3). We write the equations in dimensionless form, using for velocity βU_0 where in our physical problem U_0 is the speed of the freestream and βU_0 is the speed of the flow in the spanwise direction (rolling over the edge of the flap). Here β is typically of order unity and is to be determined later. For the dimension of length we use D, the thickness of the flap, and for the mass, ρ_0D^3. Our measurements, see Refs. 1 and 4, show correlations with lengths of order D in the span direction. We suppose from the known characteristics of the vortices generated by separation, and from the physics of the problem, that

$$A=\beta U_0D^{1/3} \qquad \Gamma/2\pi=\beta U_0D \tag{4b}$$

setting the constants of proportionality equal to 1. It will be noted that we retain but one adjustable parameter, β, thus limiting the (sometimes suspect) freedom to adjust the theory to the experiments. The equations may be conveniently made dimensionless by setting $A=\Gamma/2\pi=\rho_0=1$. Equation (4a) then becomes

$$W(\lambda)=-\lambda+i\ell n[(\lambda-\lambda_0^*)/(\lambda-\lambda_0)] \tag{5}$$

To avoid notational proliferation we use the same notation for dimensional and for dimensionless quantities; the latter may be identified by the apparent failure of dimension checks.

We find the components of the velocity in the physical plane in the usual way:

$$\dot{y}_1-i\dot{y}_2=\frac{dW}{d\lambda}\frac{d\lambda}{dz}=[-1+i(\lambda-\lambda_0^*)^{-1}$$
$$-i(\lambda-\lambda_0)^{-1}]\,\tfrac{2}{3}e^{i2\pi/3}z^{-1/3} \tag{6}$$

In the absence of the vortex the flow is steady and from Eq. (6) (without the vortex terms) we see the speed falls off as $R^{-1/3}$. The flow becomes time dependent with a vortex present because the vortex moves. Its motion is essentially the velocity of its center as determined by the potential flow and the image vortex plus a correction term, according to Routh's rule (see Ref. 8); we find

$$\dot{y}_{01}-i\dot{y}_{02}=\left\{[-1+i(\lambda-\lambda_0^*)^{-1}]\frac{d\lambda}{dz}-\frac{i}{2}\frac{d^2\lambda}{dz^2}\Big/\frac{d\lambda}{dz}\right\}_{z=z_0} \tag{7}$$

taking real and imaginary parts,

$$\begin{Bmatrix}\dot{y}_{01}\\ \dot{y}_{02}\end{Bmatrix}=\frac{2}{3}\left\{-R_0^{-1/3}+\left[R_0\sin\frac{2}{3}(\theta_0+\pi)\right]^{-1}\right\}\begin{Bmatrix}\cos 1/3\,(2\pi-\theta_0)\\ -\sin 1/3\,(2\pi-\theta_0)\end{Bmatrix}$$
$$+(6R_0)^{-1}\begin{Bmatrix}\sin\theta_0\\ -\cos\theta_0\end{Bmatrix} \tag{8}$$

where upper and lower quantities go together. We solve Eq. (8) numerically (Fig. 4); note that the solution depends upon the initial position of the vortex. In our case we take $t=0$ when the vortex crosses the symmetry line, $\theta_0=-45$ deg. The orbit (a) has $R_0=4$ initially; the orbit (b) has $R_0=2$ initially and shows the vortex moving more slowly than (a) because of the retarding effect of the vortex image; the orbit (c) approaches the wall closely enough so that the vortex is returned upstream and does not circumnavigate the corner; the orbit (d) shows the vortex close enough to the wall so that it moves counter to the motion of the potential flow. Orbits farther out show rapidly reducing sound fields: closer orbits return upstream and do not produce important characteristics of the flow. We might introduce additional vortices on the chosen orbit to model the flow process. We would introduce them at a rate equal to the peak frequency observed in the sound field. We measured (see Refs. 1, 4, and 5) the cross correlation of the surface pressure with the radiated sound pressure. In Appendix B we show that oscillations in the correlation function can be used to determine this peak frequency.

III. Aerosound Generated by Corner Flow

First note that Eq. (2) in dimensionless form becomes

$$\rho-1=\frac{Cx_i}{4\pi a_0^3x^2}\left[\delta_{i2}\frac{\partial}{\partial t}\int_{-\infty}^{0}(p_1+p_2)\,dy_1\,|_{y_2=0}\right.$$
$$\left.-\delta_{i1}\frac{\partial}{\partial t}\int_0^{\infty}(p_1+p_2)\,dy_2\,|_{y_1=0}\right] \tag{9}$$

The pressure for inviscid flows is given by

$$p=K-\tfrac{1}{2}|u|^2-\frac{\partial\phi}{\partial t}, \quad \text{with} \quad p_1=-\frac{\partial\phi}{\partial t}$$
$$p_2=-\tfrac{1}{2}|u|^2, \qquad u=\dot{y}_1\hat{\imath}+\dot{y}_2\hat{\jmath} \tag{10}$$

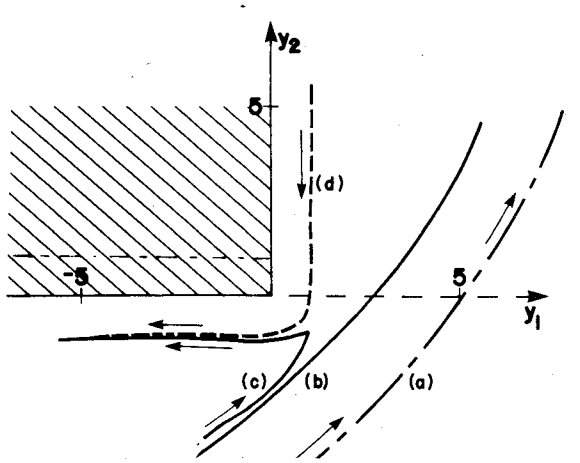

Fig. 4 Various orbits for a vortex imbedded in potential flow about a corner: (a) a vortex passing with $R_0=4$ at $t=0$ ($\theta_0=-45$ deg); (b) a vortex passing with $R_0=2$ at $t=0$; (c) a vortex turned back upstream by its image, (d) a vortex counter-circulating under the influence of its image. The divisions between the three flow regimes lie between (b) and (c) and between (c) and (d), respectively.

The force exerted on the fluid by the boundary [components P_i in Eq. (2)] is given by the pressure force normal to the surface.

Note that the positive direction for the field point $\boldsymbol{x}$ is downward and to the left, left being upstream in the flow, as indicated in Fig. 3a. In such two-dimensional problems the pressures and velocities are independent of the coordinate direction along the edge of the flap, that is, normal to the page in Fig. 3a. Consequently the surface integral along that direction is simply the (nondimensional) chord length C as indicated by the coefficient in Eq. (9). In Eq. (10) $\hat{i}$ and $\hat{j}$ are unit vectors along the axes. For this flow the velocity potential is obtained from

$$\phi = \mathrm{Re}W \tag{11}$$

where Re stands for real part, and Im, below, for imaginary part. Using Eqs. (5) and (11) we have

$$\frac{\partial \phi}{\partial t} = -2\mathrm{Im}\left[(\lambda-\lambda_0)^{-1}\frac{\partial \lambda_0}{\partial t}\right] \tag{12}$$

Note that the time dependence is contained entirely in the position of the vortex in the physical plane, z_0, or equivalently in its position in the transformed plane, λ_0. For the integrals we need, see Eq. (9), the derivative of the pressure which from Eqs. (10) and (12) is

$$\frac{\partial p_1}{\partial t} = 2\mathrm{Im}\left[(\lambda-\lambda_0)^{-2}\left(\frac{\partial \lambda_0}{\partial t}\right)^2 + (\lambda-\lambda_0)^{-1}\frac{\partial^2 \lambda_0}{\partial t^2}\right] \tag{13}$$

Think of substituting Eq. (13) for the derivative of p_1 in Eq. (9) (note that the derivatives of λ_0 are parameters in the integration). Both integrals of the second term in Eq. (13) will be divergent, referring to Eq. (5). Of course we might cut off the integrals by recognizing that the compactness of the source is violated for z sufficiently large. But if so these terms would dominate the result, being dependent as would be the case on a length of order the wavelength of the sound, or the distance to the field point, both much larger than other lengths in the calculation. This would not yield a sensible physical result for the radiated sound.

But the volume has a correspondingly divergent contribution (see the discussion in Appendix A) just cancelling this surface contribution. Accordingly we drop the second term in Eq. (13).

We designate the contribution of p_1 to the density change by $(\rho-1)_1$. The integrals involved are of elementary form.

We find for this part of the density change,

$$(\rho-1)_1 = \frac{3Cx_i}{8a_0^3x^2}\left\{\delta_{i2}\mathrm{Re}\left[\left(\frac{\partial \lambda_0}{\partial t}\right)^2\lambda_0^{-1/2}\right] - \delta_{i1}\mathrm{Im}\left[\left(\frac{\partial \lambda_0}{\partial t}\right)^2\lambda_0^{-1/2}\right]\right\} \tag{14}$$

Turn now to the pressure contribution from velocity changes, designated p_2 [see Eq. (10)].

For this contribution of the surface pressure p_0 to the dipole surface sound we need the square of the fluid velocity. Of course, by construction, the normal component of fluid velocity will vanish on the horizontal and vertical surfaces.

We take the square of the absolute value of Eq. (6); since after integrating the pressure we must take the time derivative, we may neglect the term independent of λ_0. It is seen that all of the integrals may be evaluated using standard contour integration methods. We find for the pressure integrals over the surface the result

$$\frac{\partial}{\partial t}\int_{-\infty}^{0} p_2(y_1, y_2=0)\,dy_1 + i\frac{\partial}{\partial t}\int_0^{\infty} p_2(y_1=0, y_2)\,dy_2 = \frac{\partial}{\partial t}\left[\lambda_0^{-1/2}(4i - 2i\lambda_{0i}^{-1} + \lambda_0^{-1})\right] \tag{15}$$

where $\lambda_0 = \lambda_{0r} + i\lambda_{0i}$.

Substituting and drawing these results together we have for the density change in the sound field the results, in dimensionless form,

$$\rho - 1 = [C\sin\Theta/(a_0^3 x)]\,[G_H\cos\Phi + G_V\sin\Phi] \tag{16}$$

with

$$-G_H = F_{1H} + F_{2H'}, \qquad -G_V = F_{1V} + F_{2V}$$

$$\begin{pmatrix} F_{1H} \\ F_{1V} \end{pmatrix} = \frac{u_0^2}{6R_0}\begin{pmatrix} \cos[2\phi_0 + \theta_0] \\ -\sin[2\phi_0 + \theta_0] \end{pmatrix} \tag{17}$$

$$\begin{pmatrix} F_{2H} \\ F_{2V} \end{pmatrix} = u_0(9R_0^{4/3})^{-1}\left\{(-2+\lambda_{0i}^{-1}) \times \begin{pmatrix} -\cos[\tfrac{1}{3}(\pi+\theta_0) - \phi_0] \\ \sin[\tfrac{1}{3}(\pi+\theta_0) - \phi_0] \end{pmatrix} + \frac{3}{2}R_0^{-1/3}\begin{pmatrix} -\sin(\phi_0 - \theta_0) \\ \cos(\phi_0 - \theta_0) \end{pmatrix} + \frac{2}{\lambda_{0i}}[\cos\phi_0 + \sin\phi_0\cot\tfrac{2}{3}(\pi+\theta_0)]\begin{pmatrix} -\cos\tfrac{1}{3}(\pi+\theta_0) \\ \sin\tfrac{1}{3}(\pi+\theta_0) \end{pmatrix}\right\} \tag{18)(19}$$

$$\phi_0 = \tan^{-1}(\dot{y}_{02}/\dot{y}_{01}) - \theta_0 \tag{20}$$

$$u_0 = (\dot{y}_{01}^2 + \dot{y}_{02}^2)^{1/2} \tag{21}$$

Here ϕ_0 is the angle between the vortex velocity vector, which lies in the first quadrant, and the vortex radius vector. In Eqs. (17-19) upper and lower values go together, respectively. The angle Θ here is the polar angle measured from the (outboard) corner of the flap edge; Φ is the azimuthal angle. The senses of the angles are indicated in the sketch, Fig. 2. We also show there the axes and their senses for the field vector x. The application of most interest here is that of a flap deployed from a wing surface. We have then approximately $\Phi = 0$, and $\Theta = (0, \pi)$, being zero when the field point is upstream. For this application the dipole sound generated by the edge, of width D, of the flap surface (what we have termed the vertical-surface contribution) will vanish, as we see from Eq. (16) with $\Phi = 0$. We concentrate our attention on this simplified case.

The surface pressure, p_0, is readily found using Eq. (10), substituting using Eqs. (6) and (11) for the velocity potential. The result is, up to an arbitrary hydrostatic pressure, on the surface [where by Eq. (3) we see that λ is real]

$$p_0 = -2(9R^{1/3})^{-1}[-1 + 2\lambda_{0i}|\lambda - \lambda_0|^{-2}]^2 + \frac{4u_0}{3R_0|\lambda-\lambda_0|^2}[\lambda\lambda_{0i}\cos\phi_0 + \lambda\lambda_{0r}\sin\phi_0 - |\lambda_0|^2\sin\phi_0] \tag{22}$$

The pressure due to the potential flow alone may be obtained by letting R_0 be indefinitely large. In our pressure plots in the next section we use this pressure as the reference.

As suggested earlier, in our model we may use a series of vortices, essentially set up by the separation process but, in the nature of the geometry, reaching back upstream from the separation point. These vortices are, from measurements in Refs. 1 and 4, found to be essentially, statistically independent of one another; thus we can add intensity effects. The instantaneous sound intensity at a distance x from the corner is easily found to be, now using βU_0, D, and ρ_0 to define the dimensions (for one vortex)

$$I = \frac{(\beta U_0)^6 \rho_0 C^2}{x^2 a_0^3}\sin^2\Theta\,[G_H\cos\Phi + G_V\sin\Phi]^2 \tag{23}$$

The mean intensity is found by averaging this function over the period of the vortex shedding and including the overlap of the tails of the other vortex functions which may occur. In our

applications, and in general for directly overhead, flyover flap noise, we take as indicated $\Phi = 0$, $\Theta = (0, \pi)$, see Fig. 2. In the result, Eq. (23), the quantities G_H and G_V are universal functions of dimensionless arguments varying only with the initial position of the orbit of the vortex. Even this position, as discussed, may not be widely varied.

IV. Computation Compared with Experiments

The computations required for the theory described here are not extensive. What we report was done conveniently on a hand calculator.

The vortex orbits shown in Fig. 4, calculated using Eq. (8), emphasize regions nearer to the corner. Generally speaking, when $R_0 \gg 1$, we no longer expect the model to represent the important characteristics of the physical flow, so the orbits then are not of interest; we do not show those portions. A further comment or two on the orbits will be helpful. We shall choose the orbit (b) as the one with the qualitative characteristics for the radiated sound most closely approaching the observed ones. There is a metastable point for the vortex at $R_0 \simeq 1.4$ and $\theta_0 = -45$ deg; the vortex (b) approaches this point, oscillates slightly near it (not seen on the scale of Fig. 4) and then is sent back upstream. As explained, in these pressure plots we choose $t = 0$ when the vortex passes the line $\theta = -45$ deg.

Consider the near-field pressure p_0 calculated using the orbit information already discussed and Eq. (22). We show p_0 in Fig. 5 (using the right-hand vertical scale). The pressure is measured on the surface at the point $y_1 = -0.5$, $y_2 = 0$. This position corresponds roughly to our flap measurement positions in the experiments reported in Refs. 1, 4, and 5. We show the surface pressure in Fig. 5 for orbits (a) and (b). The larger orbit shown in the figure, indicated by $R_0 = 4$, shows a single peak in time, along the horizontal axis (all quantities in dimensionless form).

As the vortex approaches the surface point, the potential flow is modified by the vortex flow. The velocities at the surface are reduced and the pressure increases. (It should be noted that we have taken for the pressure reference the potential flow value with no vortex, at the point in question. It amounts, in dimensionless form, to adding 0.35 to the calculated values.) The more interesting surface pressure for the closer orbit (b) is also shown in the figure. It is noted that there are two peaks; they appear for the following reason: As the vortex approaches the surface, the combination of it with its image reduces the flow speed (by cancelling some of the potential flow), thus increasing the pressure. As the vortex moves past the bisecting line, the images are poorly defined and the result is a reduction in the pressure because of the increased fluid velocities at the measuring point. Then as the vortex passes the corner the image again becomes better defined and a corresponding increase in pressure is seen again. It should be noted here that the speed of the vortex is considerably slowed by the action of its images. Consequently, the time of occurrence of these effects is relatively large, as can be seen in the dimensionless forms and as shown in Fig. 5; thus in dimensionless form the time delay between the two peaks mentioned here is approximately 25 units.

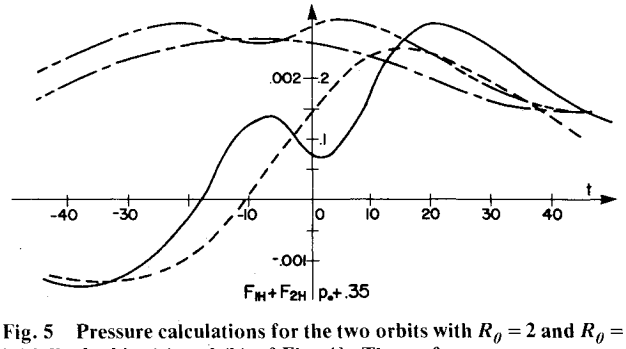

Fig. 5 Pressure calculations for the two orbits with $R_0 = 2$ and $R_0 = 4$ initially [orbits (a) and (b) of Fig. 4]. The surface pressures, p_0, are plotted using the scale on the right side of the vertical axis and are measured at $y_1 = -0.5$ and $y_2 = 0$, on the flap surface; the pressure when the vortex is distant is used as reference. The quantity $F_{1H} + F_{2H}$, proportional to the radiated sound pressure, see Eq. (16), is plotted using the vertical scale to the left; (—·—) p_0 for orbit (a); (——) p_0 for orbit (b); (---) is proportional to p for orbit (a); and (——) is proportional to p for orbit (b).

This last characteristic leads to an interesting conclusion from this work for general fluid flows. The time characteristic just described is the inverse of the Strouhal, *St*, number. As is known, *St* numbers are typically less than 1 for many flows, sometimes considerably less. The vortex street behind a cylinder has a *St* number of 0.2, a dimensionless period of 5. The reason for such low *St* numbers may in general be the phenomenon observed here: The vortex image slows the vortex motion, thus increasing the period of the fluctuating process.

Turn now to the aerodynamic sound generated by these fluctuating pressures. We show in Fig. 5 the dimensionless and normalized density change, see Eq. (16),

$$(\rho - 1)a_0^3 x/(C\sin\Theta) = G_H = -(F_{1H} + F_{2H}) \tag{24}$$

This is proportional to the density change for $\Phi = 0$. Thus we observe the sound in the plane of the flat edge. This is approximately the plane in which most of our measurements have been made. [Also note the change of sign, in Eq. (24), in the sound field density.] Radiated sound for the farthest orbit (a) shows one negative and one positive peak, widely spaced and very broad. This orbit does not approximate well the vortex activity around the flap edge. We shall emphasize the closer orbit, (b), calculations for which are also shown in Fig. 5.

For this preliminary application of the theory to the available data we restrict to but one vortex. Referring to Fig. 5, in the orbit $R_0 = 2$ we see an oscillation in p_0 noted above. New vortices must appear (not being discussed here) with a period something like this oscillation. Thus, for estimation purposes, we estimate a pressure variation with a value peak to peak, see Fig. 5, of about 0.05. This would give an rms pressure normalized by dynamic pressure (which introduces another factor of 2) of

$$p_0'/(\tfrac{1}{2}\rho_0 U_0^2) = 0.025\beta 2^{-\frac{1}{2}} \times 2 = 0.035\beta^2 \tag{25}$$

recalling that our pressure is normalized using βU_0, the spanwise flow speed. The values measured in Refs. 4 and 5 show that p_0 was approximately proportional to U_0^2, as predicted here. The normalized coefficients there ranged from

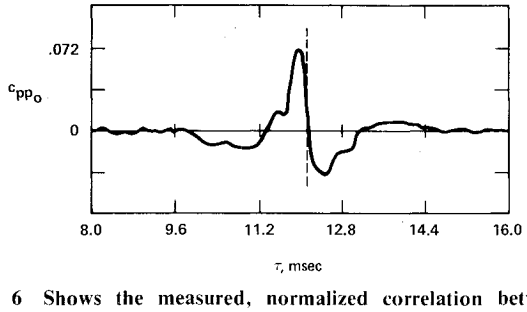

Fig. 6 Shows the measured, normalized correlation between a surface sensor placed on the outboard edge of the first flap, in a triple-flap experiment described in Refs. 4 and 5, correlated with a far-field microphone located approximately normally to the lower flap surface.

0.026 to 0.059 in typical circumstances. Obviously the theory fits these experiments quite well. It is difficult to determine the value of β, the spanwise flow intensity, from this portion of the experiment without further treatment of the additional vortices in the problem (a quasivortex street).

Our sound measurements in Refs. 1, 4, and 5 were of cross correlations between p_0, the surface, near-field, hydrodynamic pressure, and p the radiated sound pressure. Consider our large-scale 40×80-Foot Wind Tunnel experiments, see Refs. 4 and 5. In Fig. 6 we show one measured cross correlation. The random fluctuation underlying the correlation peaks is due to the high levels of extraneous noise within the wind tunnel. That background could be removed by taking considerably longer time records during the correlation process. With the funds available we were satisfied with the results shown. The thickness of the flap producing the correlation shown in Fig. 6 is approximately 3.2 cm. The freestream speed was $U_0 = 39.5$ m/s. The surface sensor was placed at midchord on the first, upstream flap. The far-field microphone for the measurement was located approximately perpendicular to the lower flap surface, in our notation $\theta \simeq 90$ deg. Figure 6 shows that the normalized cross-correlation coefficient is quite small, because of the large background noise levels. There is qualitative resemblance between this cross correlation and predicted double peak radiated sound, the negative of the $R_0 = 2$ curve shown in Fig. 5. The duration time for the double peak effect is longer, by a factor of 5 or more, than that measured. To introduce other parameters in the model flow (e.g., shaping the underlying potential flow in the transformed plane) would require other velocity or length scales in the physical flow problem, and at first it seems that none are available. But recalling, for example, flow around a cylinder, we know that behind the object, for $Re < 60$, there is a pair of vortices bound to the vicinity of the surface—a recirculation. For higher Re (Reynolds number) the vortices are shed and a street is formed. One way of looking at this is as follows: Only a weaker vortex can escape the surface and be shed into the street. Thus, in modeling the flow, using an inviscid fluid model, we see that the Reynold's number influences the qualitative characteristics, namely, as Re increases the effective vortex strength decreases. It is granted that our present Reynolds numbers are considerably larger than those for those flow regimes. Nevertheless, a way out of the paradox above is to adopt the view that even at higher Re there is a weakening of the vortex strength relative to the flow. It is not difficult to see from Eq. (8) that such a weakening reduces the image-binding effect on the vortex and speeds up the passage time about the corner.

The intensity of the radiated sound was determined in Ref. 4 using three different theoretical methods, which agreed fairly well with one another. We shall use here for reference one of these methods, based upon the surface pressure fluctuation p_0. The results for the particular flap being discussed here are shown in Table 1, refer to Eq. (23). We have $\Phi = 0$, $\theta \simeq 90$ deg; from the experiment $x_3 = 4$ m, $a_0 = 340$ m/s, $C = 0.18$ m, and $\rho = 1$ kg/m^3. The value of G_H, the negative of the plot in Fig. 5 for the curve $R_0 = 2$, is hard to determine without adding further vortices. We take as a nominal figure the peak value of about 0.003. Using the values cited, for the three flow speeds shown in Table 1 we obtain the values of $\beta^3 G_H$ shown in the last column. Evidently the values are slightly high. There are some modifications of the methods used to determine the radiated sound field in Ref. 5, which improve the comparison.

Table 1 Radiated sound as measured in the experiment of Refs. 4 and 5 from an outboard flap edge for the upstream, deployed flap

U_0, m/s	SPL at surface, dB	p' rms value of p,[4] dB	$\beta^3 G_H$ from experiment
39.5	120	63	0.003
55.8	128	77	0.006
79.0	130	85	0.005

V. Conclusions

We may sum up as follows: The computations are not extensive for the simple vortex model proposed here. We use but one truly free parameter. The theory predicts surface pressure fluctuations well.

The predicted intensity, of the radiated sound field, agrees fairly well with the experiments although it is a little low. Time characteristics of the radiated field match within an order of magnitude but show somewhat slower variation for the theory than is seen experimentally. It is believed that this can be improved by Re effects on vortex strength. It was noted in the treatment that Strouhal numbers less than 1 should be expected in general for flow phenomena of the general class considered here because of the retarding effect of vortex images upon vortex motion. The double peaks appearing in the local and radiated pressure for orbit (b) (in Fig. 5) appear to come from the presence of vortex images when the vortex lies near either one of the faces making up the corner. The lack of such well-defined images, as the vortex moves past the bisector of the corner, increases the surface pressure.

To compare properly with the sound angular directivity observed in experiments it would be necessary to introduce diffraction effects. The presence of the wing can be expected to enhance the normal dipole sound radiated in the upstream direction. This was observed in our experiments, see Ref. 5, and was earlier predicted, see Refs. 16 and 17. The diffraction effect has been recently confirmed in laboratory experiments, see Ref. 18.

Appendix A: Sound Calculations and Incompressible Flow

Lighthill,[12] after some manipulation with the exact equations of fluid motion, produces the basic wave equation with source given in Eq. (1).

In the process of derivation, Lighthill subtracted the quantity $a_0^2 \nabla^2 \rho$ from both sides of the equation. Here a_0, with dimensions of speed, is an arbitrary parameter in the development. No matter what speed is used, the correct result must be obtained when the fluid is compressible. In the usual problem one of course chooses a_0 to be the ambient speed of sound. We make use of the arbitrariness of a_0 in the discussion below.

Curle,[13] using the known solution for the wave equation with source, after some manipulation produces the exact result in dimensional form

$$\rho - \rho_0 = (4\pi a_0^2)^{-1} \left\{ \frac{\partial^2}{\partial x_i \partial x_j} \int_v T_{ij}\left(y, t - \frac{r}{a_0}\right) \frac{\mathrm{d}y}{r} - \frac{\partial}{\partial x_i} \int_s P_i\left(y, t - \frac{r}{a_0}\right) \frac{\mathrm{d}S(y)}{r} \right\} \tag{A1}$$

The first term is the usual volume sound; the second, the surface sound; and

$$P_i = -\ell_j P_{ij} \tag{A2}$$

with ℓ_i the direction cosines of the outward normal from the fluid. For our discussion it is supposed now that we have a flow of a slightly compressible fluid, permitting the true speed of sound for that fluid to increase without limit, thus approaching an incompressible flow; but suppose that for the calculation of Eq. (A1), the parameter a_0 remains fixed at some finite, fictitious value. The result will be that the left-hand side, the density change of Eq. (1), approaches zero. We use the incompressible flow quantities to calculate T_{ij} and P_i. The result is evidently that the two integrals in Eq. (A1) are equal and opposite. The two types of aerosound just cancel

one another. To re-emphasize, we expect (using incompressible flow quantities in an aerosound calculation with a fictitious, finite speed of sound) that the surface and volume sound contributions just cancel one another. This result has been checked in at least one situation and found to hold, see Lauvstad and Meecham.[15] In that work a cylinder oscillating (rotating) about its axis and imbedded in an incompressible, viscous fluid produces the expected cancellation.

Appendix B: Relation Between Correlation Width and Spectrum Maximum

Consider a model, broad-band energy spectrum given by

$$E(\omega) = e^{-(\omega-\omega_m)^2/\omega_m^2} + e^{-(\omega+\omega_m)^2/\omega_m^2} \tag{B1}$$

where ω_m is of order the angular frequency of the spectrum maximum. The correlation function is found by taking the Fourier transform,

$$R(t) = \int e^{i\omega t} E(\omega)\, d\omega \tag{B2}$$

The normalized auto correlation is thus

$$R(t)/R(0) = \cos(\omega_m t)\exp\{-t^2\omega_m/4\} \tag{B3}$$

We note that even though a Gaussian spectrum centered at the origin has a monotonic correlation function, such a spectrum displaced from the origin has an oscillating correlation function. This is generally true; a spectrum with a maximum displaced from $\omega = 0$ (the typical result in experiments of our kind) will have an oscillating correlation function. No physical model is necessary to explain the observed correlation oscillations.

Acknowledgments

This work was supported by the NASA Ames Research Center. The author is indebted to N. M. Nguyen-Vo for the computations presented here.

References

[1] Ahtye, W. F., Miller, W. R., and Meecham, W. C., "Wing and Flap Noise Measured by Near- and Far-Field Cross-Correlation Techniques," AIAA Paper 79-0667, 1979.

[2] Fink, M. R. and Schlinker, R. H., "Airframe Noise Component Interaction Studies," NASA CR-3110, March 1979.

[3] Kendall, J. M. and Ahtye, W. F., "Noise Generation by a Lifting Wing/Flap Combination at Reynolds Numbers to 2.8×10^6," AIAA Paper 80-0035, Jan. 1980.

[4] Miller, W. R., Meecham, W. C., and Ahtye, W. F., "Large Scale Model Measurements of Airframe Noise Using Cross-Correlation Techniques," UCLA Report, Feb. 1981; see also *Journal of the Acoustical Society of America,* Vol. 71, Pt. 3, 1982, pp. 591-599.

[5] Miller, W. R., "Flap Noise Characteristics Measured by Pressure Cross-Correlation Techniques," Ph.D. Thesis, University of California at Los Angeles, Los Angeles, Calif., 1980.

[6] Hayden, R. E., "Noise from Interaction of Flow with Rigid Surfaces; A Review of Current Status of Prediction Techniques," NASA 1-9559-14, Jan. 1972.

[7] Yu, J. C. and Tam, C. K. W., "An Experimental Investigation of the Trailing Edge Noise Mechanism," AIAA Paper 77-1291, 1977.

[8] Clements, R. R., "An Inviscid Model of Two Dimensional Vortex Shedding," *Journal of Fluid Mechanics,* Vol. 57, Pt. 2, 1973, pp. 321-336.

[9] Howe, M. S., "Contributions to the Theory of Aerodynamic Sound, with Application to Excess Jet Noise and the Theory of the Flute," *Journal of Fluid Mechanics,* Vol. 71, Pt. 4, 1975, pp. 625-673.

[10] Howe, M. S., "The Influence of Vortex Shedding on the Generation of Sound by Convected Turbulence," *Journal of Fluid Mechanics,* Vol. 76, Pt. 4, 1976, pp. 711-740.

[11] Hardin, J. C., "Noise Radiation from the Side Edges of Flaps," *AIAA Journal,* Vol. 18, May 1980, pp. 549-552.

[12] Lighthill, M. J., "The Bakerian Lecture, 1961: Sound Generated Aerodynamically," *Proceedings of the Royal Society A,* Vol. 216, May 8, 1962, pp. 147-182.

[13] Curle, N., "The Influence of Solid Boundaries upon Aerodynamic Sound," *Proceedings of the Royal Society A,* Vol. 231, July 8, 1955, pp. 505-514.

[14] Francis, M. S. and Kennedy, D. A., "Formation of a Trailing Vortex," *Journal of Aircraft,* Vol. 16, March 1969, pp. 148-154.

[15] Lauvstad, V. R. and Meecham, W. C., "Acoustic Radiation from a Sinusoidally Rotating Circular Cylinder," *Journal of Sound and Vibration,* Vol. 10, No. 3, 1969, pp. 455-463.

[16] Yildiz, M. and Mawardi, O. K., "On the Diffraction of Multipole Fields by a Semi-Infinite, Rigid Wedge," *Journal of the Acoustical Society of America,* Vol. 37, No. 19, 1960, pp. 1685-1691.

[17] Ffowcs-Williams, J. G. and Hall, L. H., "Aerodynamic Sound Generated by Turbulent Flow in the Vicinity of a Scattering Half Plane," *Journal of Fluid Mechanics,* Vol. 90, Pt. 7, 1970, pp. 657-670.

[18] Meecham, W. C., Bui, T. D., and Miller, W. R., "The Diffraction of Dipole Sound by the Edge of a Rigid Baffle," *Journal of the Acoustical Society of America,* Vol. 70, No. 5, 1981, pp. 1531-1533.